Dynamics of the energy relaxation in a parabolic quantum well laser

A. V. Trifonov,[1,*] E. D. Cherotchenko,[2,†] J. L. Carthy,[2] I. V. Ignatiev,[1] A. Tzimis,[3,4] S. Tsintzos,[3,4] Z. Hatzopoulos,[3,4] P. G. Savvidis,[3,4] and A. V. Kavokin[1,2,5]

[1]*Spin Optics Laboratory, St. Petersburg State University, 1, Ulianovskaya, St. Petersburg, 198504, Russia*
[2]*School of Physics and Astronomy, University of Southampton, Southampton, SO17 1BJ, United Kingdom*
[3]*Department of Materials Science and Technology, University of Crete, 71003 Heraklion, Crete, Greece*
[4]*FORTH-IESL, PO Box 1385, 71110 Heraklion, Crete, Greece*
[5]*CNR-SPIN, Viale del Politecnico 1, Rome I-00133, Italy*

(Received 17 August 2015; revised manuscript received 1 February 2016; published 14 March 2016)

We explore two parabolic quantum well (PQW) samples, with and without Bragg mirrors, in order to optimize the building blocks of a bosonic cascade laser. The photoluminescence spectra of a PQW microcavity sample is compared against that of a conventional microcavity with embedded quantum wells (QWs) to demonstrate that the weak coupling lasing in a PQW sample can be achieved. The relaxation dynamics in a conventional QW microcavity and in the PQW microcavity was studied by a nonresonant pump-pump excitation method. Strong difference in the relaxation characteristics between the two samples was found. The semiclassical Boltzmann equations were adapted to reproduce the evolution of excitonic populations within the PQW as a function of the pump power and the output intensity evolution as a function of the pump-pump pulse delay. Fitting the PQW data confirms the anticipated cascade relaxation, paving the way for such a system to produce terahertz radiation.

DOI: 10.1103/PhysRevB.93.125304

I. INTRODUCTION

Recently research into coherent light sources based on bosonic systems (known as bosers, or bosonic lasers) has seen a rapid increase [1]. In contrast to conventional lasers based on the phenomenon of stimulated emission, bosonic lasers are based on stimulated relaxation of bosons and the formation of an exciton-polariton condensate [2]. This stimulated relaxation is triggered by the final state occupation of an energy level within a system, and serves as the principal tool for building up of a polariton population in a given energy state [3]. The coherence of boser radiation is the result of spontaneous emission of photons by the condensate after its occupation exceeds unity [4], making such a system ideal for a low-threshold lasing device.

In this paper we build upon the idea of a bosonic cascade laser (BCL) introduced by Liew *et al.* [5] that is capable of emitting terahertz (THz) radiation, a technologically underdeveloped section of the electromagnetic spectrum [6]. The BCL uses a cascade mechanism similar to that of the quantum cascade laser (QCL) [7,8] in order to generate radiation. Unlike the QCL, which uses multiple adjacent quantum wells (QWs) [9] as the cascade ladder, the BCL cascade [10] is formed by equidistant excitonic levels in a single parabolic quantum well (PQW) [11–16]. Although intersubband polariton QCL lasers have been proposed [17,18], these rely upon the need for population inversion between adjacent subbands, analogous to the QCL. In a BCL, however, the amplification is due to the bosonic stimulation of radiative transitions between levels in a cascade. Both the QCL and a range of other proposed microcavity systems are capable of generating THz [19–22], but the BCL uniquely offers increased amplification created by the final polariton state stimulation within the confines of *one* PQW.

In Ref. [23] we have shown that a microcavity with an embedded single parabolic quantum well exhibits optical lasing that is prerequisite for stimulated polariton relaxation in the cascade. THz frequency quantum beats in pump-probe spectra have been reported in Ref. [23]. Here we present further studies of the nontrivial polariton dynamics in bosonic cascade microcavities. We find unusual pump-power dependencies of the photoluminescence (PL) in the PQW sample without the microcavity, which we believe to be due specifically to the bosonic cascade relaxation mechanism. We compare polariton and photon lasing regimes in microcavities with rectangular and parabolic quantum wells, respectively. We also investigate the relaxation dynamics of excitons in MCs with parabolic and rectangular QWs. Using a pump-pump method, excitons are seen to relax in the PQW much faster than in a MC with a rectangular QW. We believe the accelerated relaxation in PQW to be an indication of stimulated relaxation in a bosonic cascade and find that the experimental results are in agreement with the BCL model of Ref. [5].

II. SAMPLES AND EXPERIMENTAL SETUP

A PQW sample without and with (denoted S1 and S2, respectively) Bragg reflectors (DBRs) have been studied, and their relaxation and excitation characteristics have been compared to a planar microcavity sample with rectangular QWs (S3). All samples were fabricated with molecular beam epitaxy. S1 contains an InGaAs/GaAs PQW of width $\approx$50 nm at the top of the potential well, and the parabolic profile was achieved by altering the indium concentration during the growth process from 2% at the InGaAs/GaAs interface to 6% in the middle of QW (see inset in Fig. 1). Sample S2 was fabricated similarly with an $Al_xGa_{1-x}As/Al_{0.15}Ga_{0.85}As$ QW of $\approx$ 50 nm width, where the parabolic profile was achieved by altering the concentration of aluminium along the z axis of the sample from 5% in the middle of the QW to 12% near the interface. The microcavity was formed with two DBRs,

*Corresponding author: arthur.trifonov@gmail.com
†Corresponding author: E.Cherotchenko@soton.ac.uk

 ©2016 American Physical Society

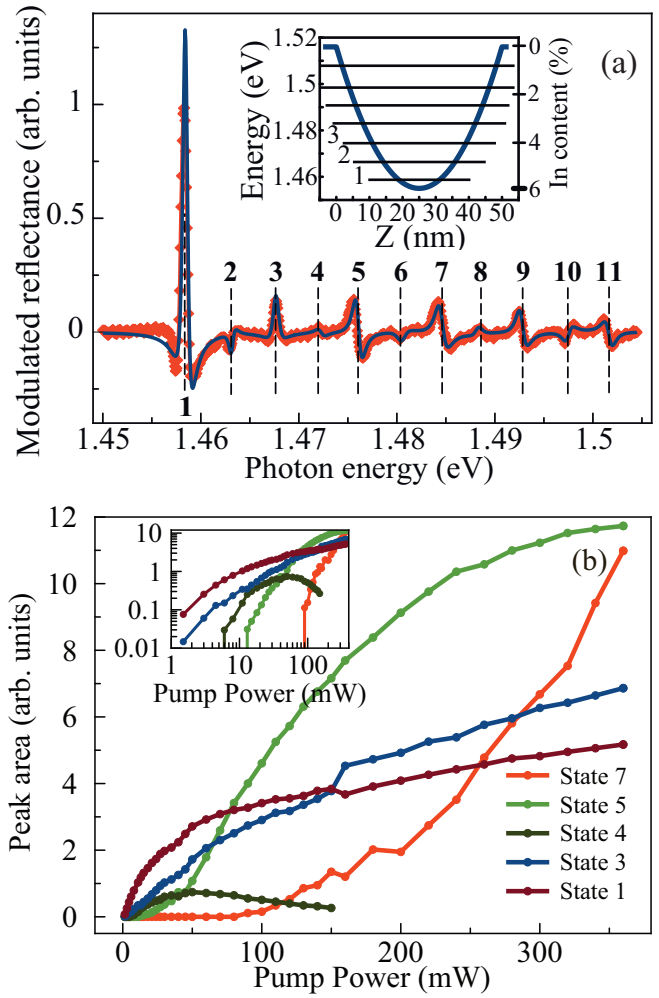

FIG. 1. (a) λ-modulated reflectivity spectrum of sample S1 containing parabolic QW without microcavity (red curve) and modeled spectrum (black curve). Vertical dashed lines mark equidistant quantum confined excitonic states in the PQW. Inset: the potential profile for excitons (left axis) and distribution of indium content across the QW layer (right axis) are shown. (b) Pump power dependencies of integral PL from different quantum confined excitonic states. The pump wavelength was tuned to the exciton resonance in the barrier layer. The integral PL for each transition was obtained by deconvolution of the PL spectra into a set of Lorentzians. The inset presents the same curves plotted in logarithmic scale to show the low power region.

each with 17 and 22 $Al_{0.15}Ga_{0.85}As$/AlAs paired layers. The Q factor of the microcavity is approximately 2000 and the PQW was placed in the middle of $3\lambda/2$ intracavity spacing.

Finally a $5\lambda/2$ planar GaAs cavity, sample S3, consisting of 32 and 35 $Al_{0.15}Ga_{0.85}As$/AlAs DBR pairs and 12 rectangular QWs was studied. The Q factor of this microcavity is approximately 12 000.

The samples were mounted in a close-cycle cryostat to reach a temperature of roughly 5 K. Samples S2 and S3 were excited nonresonantly above the microcavity stop-band by femtosecond pulses from a Ti:Sa laser. The laser spot size was approximately 50 μm. S1 was exited with a cw laser resonantly tuned to the exciton resonance in the barrier layers (to the 12th quantum confined excitonic state; see Fig. 1). Such pump conditions allowed us to create excitons rather than electron-hole pairs. To study the exciton relaxation dynamics of S2 and S3 we used a pump-pump technique, whereby two pump pulses separated by a variable delay are used to excite a sample nonresonantly with a high temporal resolution that allowed us detecting the time-integrated intensity of the PL as a function of the delay. We compare the dynamics measured in a new microcavity sample containing a single PQW (S2) with the data taken on a reference sample that is a state of the art strong coupling microcavity containing 12 embedded QWs and characterized by a Q factor of 12 000. Both sets of data may be described within the kinetic model that allows revealing the role of key parameters of microcavities, namely, the relaxation and radiative decay rates, the number of intermediate exciton subbands.

III. PQW WITHOUT MICROCAVITY

In order to realize a BCL and confirm its relaxation mechanism, we first characterized the bare PQW sample, S1, to verify that equidistant exciton states had been achieved. Therefore, S1 was assessed using sensitive λ-modulated reflection [24] and PL spectroscopy. In Fig. 1(a) the modulated reflectance spectrum is presented (red curve) and subsequently fitted (solid black line) and up to 11 distinct excitonic states can be resolved. The energy spacing between the neighboring resonances is about 6 meV, or 1.45 THz. The inset in Fig. 1(a) shows the potential profile for excitons in PQW (blue line) and the positions of equidistant quantum confined excitonic states (horizontal black lines), which creates the bosonic cascade ladder.

We performed a simple analysis of the reflectivity spectrum generalizing the theory developed in Refs. [25,26] for the case of several exciton quantum confined states to fit the modulated reflection data. The modulation technique was used to reduce a noise and to stretch weak features connected to the excited quantum confined excitonic states. Following the nonlocal dielectric response theory [25], the amplitude reflection coefficient for a QW with several exciton resonances can be written in the form

$$r_{\mathrm{QW}} = \sum_{N=1}^{N_{\max}} \frac{i(-1)^{N-1}\Gamma_{0N}e^{i\varphi_N}}{\omega_{0N} - \omega - i(\Gamma_{0N} + \Gamma_N)}. \qquad (1)$$

Here ω_{0N} is the resonance frequency; Γ_{0N} and Γ_N are the radiative and nonradiative damping rates for a system of N levels. The phase φ_N in this equation takes into account a possible asymmetry of the QW potential. Reflectivity $R(\omega)$, from the structure with a top barrier layer of thickness L_b and a QW layer of thickness L_{QW}, is calculated using the transfer-matrix approach:

$$R(\omega) = \left| \frac{r_{01} + r_{\mathrm{QW}}e^{2i\phi}}{1 + r_{01}r_{\mathrm{QW}}e^{2i\phi}} \right|^2, \qquad (2)$$

where r_{01} is the amplitude reflection coefficient from the sample surface. The phase is $\varphi = K(L_b + L_{\mathrm{QW}}/2)$, where K is the photon wave vector in the heterostructure. The calculated derivative reflectivity spectrum is shown in Fig. 1 (black curve).

The peak integrated PL spectra of the sample S1 at different excitation powers has been measured [see Fig. 1(b)]. We have found that the power increase gives rise to the increase of PL intensity from the lowest exciton state followed by its saturation, contrary to the model set out in Ref. [5] where the highest level is seen to populate first, and the lowest level establishing a population last. Simultaneously, the intensity of the PL from the excited exciton states increases superlinearly with pump power and then also saturates. The similar behavior of PL is observed for exciton states under further increase of the pump power. The full set of the PL data consisting of about 500 spectra was analyzed by deconvolution of each spectrum into a set of Lorentzian resonances, corresponding to different exciton transitons. We have found that such deconvolution fits the experimentally observed spectra, if the wavelength of excitation coincides with one of the exciton resonances in PQW or with the exciton resonance in barrier layers. In this case, the pump directly creates excitons rather than uncoupled electron-hole pairs, the relaxation of which differs from exciton relaxation. If electron-hole pairs are created by the nonresonant excitation, a broad structureless background appears in the PL spectra.

We should stress that the observed behavior of the time integrated PL intensities of resonant exciton peaks is a characteristic of PQWs. This is a clear indication that excitons created by resonant excitation relax via cascade between neighboring energy levels. We have studied by the same technique a reference rectangular QW of thickness of about 90 nm and found that no new exciton lines appear in the PL spectra with the pump power increase.

IV. PQW IN A MICROCAVITY

The ability of the parabolic quantum well sample S2 to act as a polariton laser [3] is a nontrivial question. Heterostructures acting as polaritonic lasers usually contain multiple thin QWs (of roughly 10 nm in width) to increase the oscillator strength of the excitonic transition in order to establish strong coupling. S2, however, contains just one PQW of about 50 nm width. The larger QW thickness and stronger overlap of the electron and hole wave functions in the PQW provides a sufficiently large exciton-photon coupling to make the strong coupling regime and polariton lasing possible [27]. Only the lowest energy exciton state in a parabolic QW is strongly coupled to the cavity mode in the low excitation regime. All other states are in the weak coupling regime due to the low overlap of exciton center of mass wave functions and the cavity mode.

Figure 2(a) shows the dependencies of polariton mode energies on the laser spot position on the sample S2. One can see that the detuning between the exciton and photon resonances is dependent on the spot position. The anticrossing of polariton modes is clear evidence of the strong coupling regime. In the anticrossing range the reflectivity spectrum exhibits three distinct minima, these can be attributed to the coupling of the heavy-hole and light-hole excitons [28] to the cavity mode. The Rabi splitting of the relating polariton states is about 6 meV. The light-hole exciton is considered to be weakly coupled with the cavity mode because as one can conclude from the weak dependence of the corresponding resonance feature in PL spectra on the exciton-photon detuning. The data presented in the next section has been taken at the slightly negative detuning that corresponds to the range 750–800 μm in Fig. 2(a).

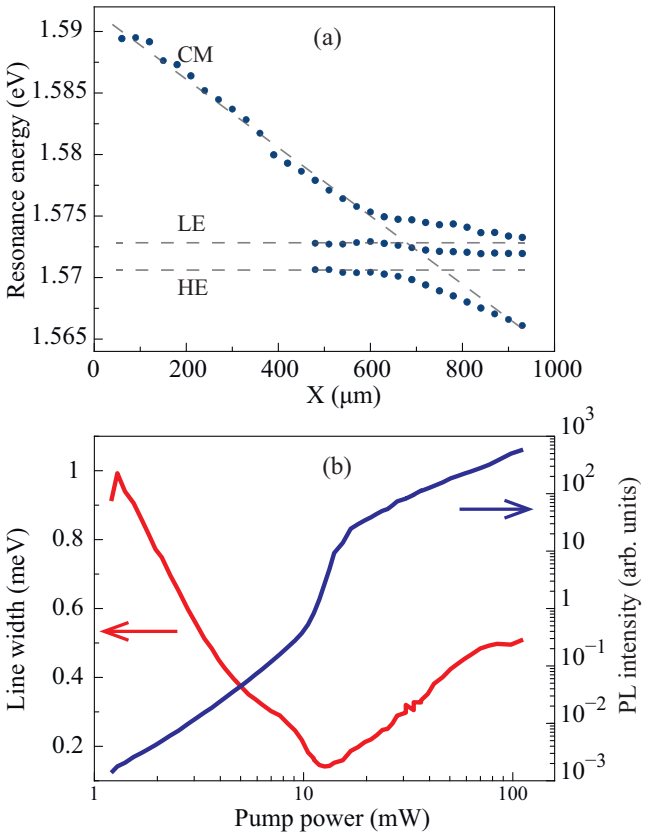

FIG. 2. (a) Energy positions of features in reflectivity spectra of the sample S2 as a function of the laser spot position on the sample (blue dots). Dashed lines marked by CM, LE, and HE are the resonant energies of the cavity mode, light-hole exciton, and heavy-hole exciton, respectively. (b) The dependencies of the PL intensity (blue curve) and PL linewidth (red curve) on the excitation power for the sample S2.

The pump-power dependence of PL intensity for sample S2 is shown in Fig. 2(b) (blue curve). The thresholdlike increase of the intensity is clearly observed. The identification of the threshold, polariton or conventional laser threshold, is questionable without additional experiments. What is important is that the PL intensity rises exponentially with the pump power below the threshold. At the pulsed excitation this is an indication of the switching of the system to the lasing regime within a limited time window, which becomes larger as the pump power increases. The linewidth narrowing at the threshold pump power is clearly seen in Fig. 2(b) (red curve). We consider it as an indication that the stimulated relaxation occurs in sample S2.

V. PUMP-PUMP EXPERIMENTS

The pump-pump method we employ allowed one to highlight relaxation processes in the PQW within the MC that may be hidden for studies by conventional time resolved spectroscopy methods due to the reflection from the DBRs [29]. The important property of the stimulated cascade relaxation is its strong dependence on population of the

lower-lying exciton state [5]. In the pump-pump method, the first pulse creates some initial density of excitons and the delayed second pump pulse creates additional excitons at the pumped level. Relaxation of these excitons strongly depends on the population of lower energy excitonic levels created by the first pump pulse. If this population is large enough, the stimulated relaxation is triggered and accelerated. This acceleration should result in the nonlinear increase of the total PL signal excited by both pump pulses in the case of competing radiative and nonradiative channels of polariton recombination. The PL intensity should depend on the delay between two pulses; no nonlinear PL increase should occur at very large delays, where the excitons created by the first pulse relax and recombine before the second pulse arrives.

We have employed the proposed method for a comparative study of two samples S2 and S3. The samples were cooled down in a cryostat to 5 K and pumped by two femtosecond pulsed beams. The time integrated PL spectra was measured as function of delay between the pulses. We intentionally use spatially large laser spots in order to reduce the effects of diffusion and lateral polariton drift. A detailed treatment of the formation dynamics of polariton condensates accounting for the drift and diffusion of photoexcited carriers and excitons is presented in the recent paper [30]. The goal of our present study is to reveal the specifics of momentum space relaxation in bosonic cascade structures. The studies of spatial dynamics of exciton clouds and polariton condensates in such structures will be subject of our future research. Figure 3 shows the delay dependencies of time integrated PL spectra of sample S2 with PQW (a) and of sample S3 with multiple rectangular QWs (b) at the pump powers $0.25P_{th} + 1.7P_{th}$, where P_{th} is the threshold pump power for each sample. $P_{th} = 16$ mW for the sample S2 and $P_{th} = 1.1$ mW for S3. The spectral diffusion as well as appearance of the additional spectral peaks are clearly observed at positive delays for both the samples. However, time scale for these processes are different. For sample S2 the second peak is developing from 30 to 50 ps, while for sample S3 it takes much longer delays, from 10 to 200 ps.

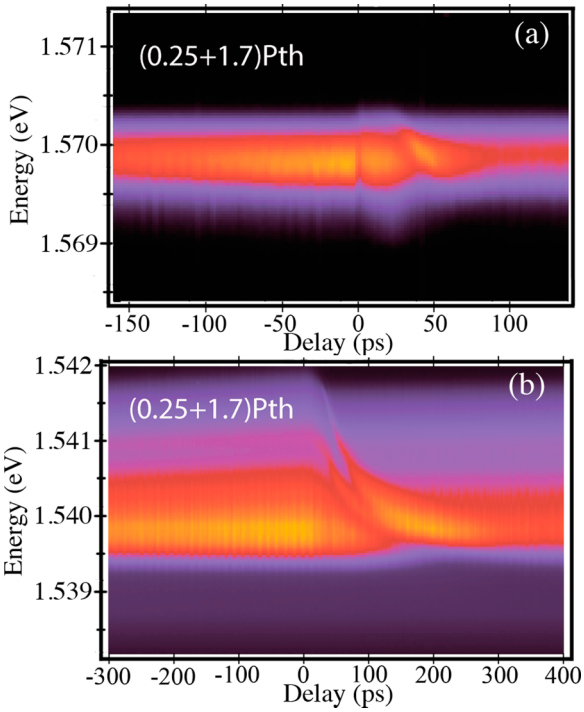

FIG. 3. PL spectra measured as a function of the delay between the pump pulses for (a) sample S2 with PQW and (b) sample S3 containing multiple rectangular QWs in a MC.

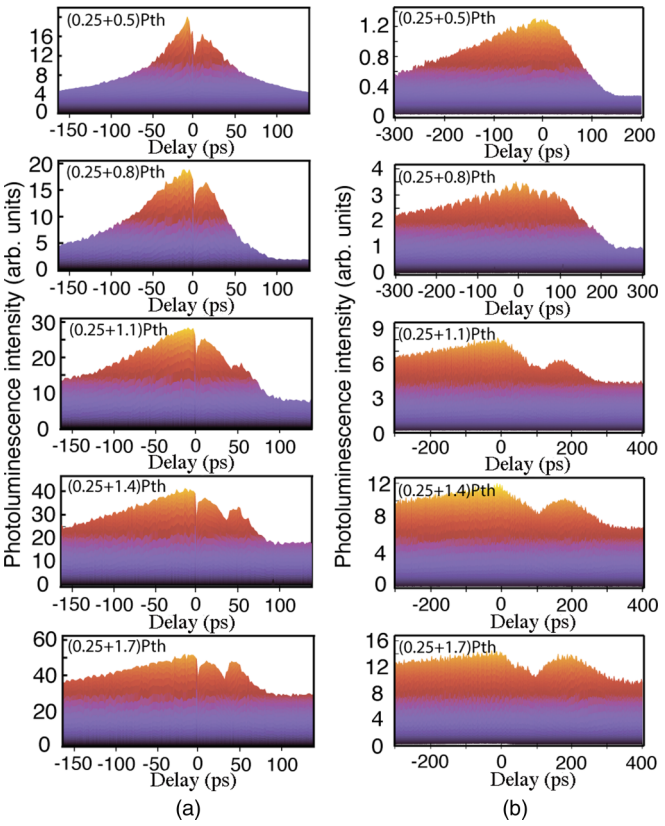

FIG. 4. PL intensity as a function of the delay between two pump pulses for different values of the pump intensities for PQW sample S2 (a) and rectangular QWs sample S3 (b). Profiles of the PL intensities corresponding to the color plot in Fig. 3 are taken at the energies $E = 1.5698$ eV for panel (a) and $E = 1.5399$ eV for panel (b).

Figure 4 shows the delay dependencies of the PL intensity measured for the samples S2 and S3 at different excitation powers of both pulses. The delay dependencies of spectrally resolved PL intensities are taken at the energies $E = 1.5698$ eV (a) and $E = 1.5399$ eV (b) corresponding to the peaks in the PL spectra; see Fig. 3. The pump powers are chosen close to the threshold of lasing. There are several peculiarities in these dependencies. First, there is a strong increase of the PL at a relatively small delay. At the same time, the range of these delays is considerably smaller for PQW (150 ps) than that for rectangular QWs (several hundred ps). This means that the relaxation processes in the PQW are considerably faster than in the rectangular QWs.

Secondly, additional features in these dependencies are observed. For PQW, a relatively narrow dip at zero delay is clearly seen. No such dip is observed for rectangular QWs. This is an indication of significant difference in relaxation processes in these two samples.

Thirdly, some asymmetry of the dependencies for positive and negative delays is observed in both samples. It is caused by the difference in pump powers of first and second pulses. If the weak pulse comes first (negative delay), the exciton population is relatively small, consequently the bosonic stimulation is weak, and the relaxation of excitons created by the weak pulse is relatively slow. When the strong pulse comes first (positive delay), the stimulated relaxation is accelerated compared to the case of a weak pulse coming first.

Finally, an additional peak of PL intensity is observed at the positive delay, if the power of the strong pulse is beyond the threshold. To understand the second peak at the positive delays one should discuss the time dependence of PL intensity. In Ref. [31], the PL kinetics has been studied at different exciting powers for both below and above the threshold of polariton lasing, P_{th}. It was found that, when the power $P < P_{th}$, the PL intensity slowly rises and reaches its maximum at $t_1 \approx 100$ ps. At later times PL intensity slowly decreases with characteristic decay time $t_2 \approx 400$ ps. When the pump power exceeds the threshold, a strong pulse of polariton laser emission appears at time t_1 with the 10–20 ps pulse duration. Such temporal behavior of PL intensity allows us to assume the following origin of second peak in the pump dependencies shown in Fig. 4. When the sample is pumped by two pulses and the first pulse power is above the threshold two maxima of the polariton laser emission may be seen. The reason is that the number of excitons remained after the first pulse of polariton lasing peak and of excitons created by the second pump pulse is sufficient for the formation of the second peak of polariton laser emission. These effects with polariton lasing appearing twice are expected to be present in the sample S2 with PQW in MC as well as in the sample S3 with rectangular QW in MC. But the time delay and the width of the second peak strongly depends on the relaxation dynamics. Thus in the sample S2 the relaxation is faster than in the sample with a rectangular QW in MC.

VI. MODELING

Exciton relaxation and dynamics in GaAs MCs has been extensively studied in conventional QWs [32–35], particularly in what concerns phonon mediated relaxation. In order to analyze the experimental data obtained for the PQW, we use the rate equations introduced by Liew *et al.* [5], using the Boltzmann kinetic theory of relaxation [36]. We consider m distinct excitonic levels in a PQW. The dynamics of population of each of the levels can be described by the following system of rate equations:

$$\frac{dN_m}{dt} = -\frac{N_m}{\tau_u} - \sum_{i=1}^{m-1} W_i N_m (N_{m-i}+1) + \frac{\alpha}{2} N_{m-1}^2 (N_m+1)(N_{m-2}+1) - \frac{\alpha}{2} N_m N_{m-2}(N_{m-1}+1), \tag{3}$$

$$\frac{dN_k}{dt} = P_k^{(1)}(0) + P_k^{(2)}(\tau_{\text{delay}}) - \frac{N_k}{\tau_p} + \sum_{i=1}^{m-k} W_i (N_{k+i}(N_k+1)) - \sum_{i=1}^{k-1} W_i N_k (N_{k-i}+1) - \alpha {N_k}^2 (N_{k+1}+1)(N_{k-1}+1) + \alpha N_{k+1} N_{k-1} \times (N_k+1)^2 + \frac{\alpha}{2} N_{k+1}^2 (N_k+1)(N_{k+2}+1) - \frac{\alpha}{2}(N_{k+1}+1)^2 N_k N_{k+2} - \frac{\alpha}{2} N_{k-1}^2 (N_k+1) \times (N_{k-2}+1) + \frac{\alpha}{2} N_{k-2} N_k^2 (N_{k-1}+1)^2, \quad k = 2 \ldots m-1, \tag{4}$$

$$\frac{dN_1}{dt} = -\frac{N_1}{\tau_g} + \sum_{i=1}^{m-1} W_i N_{i+1}(N_1+1) + \frac{\alpha}{2} N_2^2 (N_1+1)(N_3+1) - \frac{\alpha}{2} N_1 N_3 (N_2+1)^2. \tag{5}$$

Here N_1 denotes the occupation of the ground level of PQW, N_m is the occupation of the highest level, and N_k is the occupation of k level with $k = 2 \ldots m-1$; α terms describe the exciton-exciton scattering in the system. Terms $P_k^{(1)}(0)$ and $P_k^{(2)}(\tau_{\text{delay}})$ describe the initial two pulse excitation where the second pulse comes with a delay τ. Terms $-N_k/\tau_k$ for $k = 2 \ldots m$ describe both radiative and nonradiative decay rate of excitons at each level. Phonon-assisted relaxation of excitons is taken into account in these terms. For the first level, only the radiative recombination is taken into account.

Matrix elements W_i describe the transition from any level k to any other level $k-i$ in the cascade. Transitions between adjacent levels may be mediated by emission of THz radiation as suggested in Ref. [5]. We generalize this model and consider the THz transitions between all the levels, which is described in the above equations by summation over all levels.

We assume that the pumping is centered at one of the middle levels of the cascade, k, meaning that upward scattering is possible from this level. The upward scattering due to exciton-exciton interaction populates all the levels up to the highest one labeled m. For the structure under study, the exciton-exciton scattering is found to change the amplitude of the PL signal, but does not affect the most important features of the exciton dynamics. The exciton-exciton scattering plays a minor role in our experiments and the corresponding terms in rate equations can be safely omitted.

Experimentally, the system is excited by femtosecond pulses which are relatively broad in energy and capable of pumping several energy levels of the cascade simultaneously. To account for the spectral broadening of the pulse in the model, we assume that polaritons are excited not only at the level k, but also at the nearest levels $k-1$ and $k+1$. In the numerical simulations, the cascade is considered to have maximum number exciton levels $m = 9$ with level $k = 6$ receiving the major part of input pulses power, $2P/3$, and levels $k = 5$, 7, receiving 1/6 of total input power each. We have used the following parameters in the calculations: $W_1 = 1500\ \text{s}^{-1}$, $W_2 = W_4 = 500\ \text{s}^{-1}$,

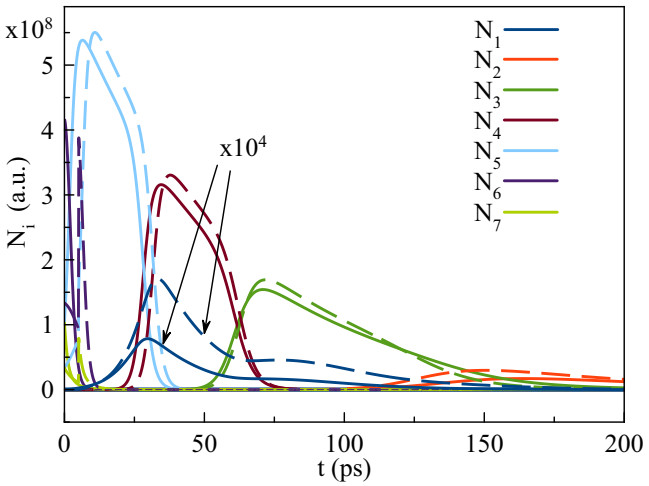

FIG. 5. Time evolution of exciton densities at each level in the QW. Solid lines are calculated for zero delay between pulses and dashed lines show the same for $\tau_{\text{delay}} = -5$ ps.

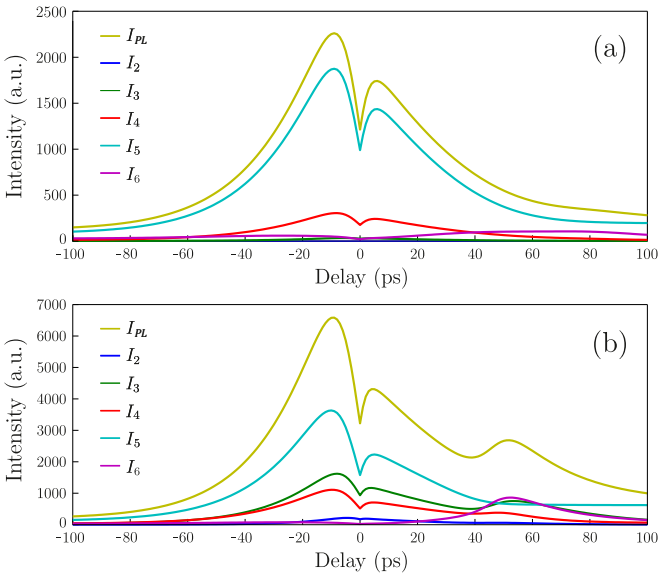

FIG. 6. Modeling of pump-pump signal with use of rate equations: delay dependencies of total PL intensity I_{PL} from the ground exciton level, and separate contributions of each transition $I_i = W_{i-1}N_i(N_1 + 1)$ for $i = 2 \ldots 6$, plotted for two different values of pump powers: (a) $P^{(1)} = 0.3 \times P_{Thr}$, $P^{(2)} = 0.25 \times P_{Thr}$ and (b) $P^{(1)} = 0.7 \times P_{Thr}$, $P^{(2)} = 0.25 \times P_{Thr}$.

$W_3 = 100\ \text{s}^{-1}$, $W_5 = 2500\ \text{s}^{-1}$, $\tau_g = 11$ ps, $\tau_p = 55$ ps, and $\tau_u = 22$ ps. where τ_g, τ_u, τ_p are the decay times for the ground level, pumped levels, and levels above the pumped one, respectively.

Figure 5 shows the time evolution of exciton densities at each energy level in the QW, plotted for two different delays between the pulses. As seen from the figure, the population dynamics is quite complex. If the system is excited by a single pulse (solid lines in Fig. 5), pumped levels 5–7 are populated and other levels are almost empty at the initial time interval ($t < 10$ ps) after the pulse. Due to the high exciton density at the level 5, $N_5 \gg 1$, the Bose-stimulated relaxation from the upper levels 6 and 7 is switched on and the population of this level dramatically increases. The population of level 5 reaches its maximum at $t \approx 5$ ps, while levels 6 and 7 become empty. The low-lying levels, $i = 4 \ldots 1$, are slowly populated while the exciton density is not reached a critical value for Bose-stimulated relaxation. This critical value is achieved for the level 4 first because, in the framework of our model, the relaxation between adjacent levels is more efficient, $W_1 > W_2, \ldots, W_4$. This explains the thresholdlike increase of population of the level 4 at time $t \approx 30$ ps. Similarly, populations of levels 3 and 2 rapidly increase at time $t \approx 60$ ps and $t \approx 120$ ps, respectively (see respective curves in Fig. 5). However, the population of the lowest exciton level, 1, is not efficiently boosted via this pathway because of the low population of the adjacent level 2. Therefore, we have to assume in our model that there is a direct relaxation of excitons from the pumped level 5 to the lowest level. As we will see below, this process explains the second maximum observed experimentally in pump-pump experiments [see Fig. 4(a)].

Nonradiative losses of excitons, described by terms $-N_i/\tau_j$ in Eqs. (3)–(5), compete with the relaxation processes. The integral magnitude of losses depends on the time, spent by excitons at the excited levels. This time can be drastically shortened and, correspondingly, the PL yield can be increased, if appropriate experimental conditions initiating the Bose-stimulated relaxation are fulfilled, in particular, the excitation power, which should be close to the threshold power for polariton lasing [37]. Separation of the excitation pulse in two pulses also helps controlling the population of different exciton levels (see Fig. 5) and, hence, the nonradiative losses. Once the excitons created by the first pulse have relaxed to the fifth level (it takes about 5 ps), the excitons created by the second pulse delayed by $\tau = 5$ ps rapidly relax from the sixth and seventh levels to the fifth one via Bose-stimulated process. This stimulation gives rise to the increased population of level 5 relative to that obtained for zero delay, as one can conclude comparing solid and dashed lines N_5 in Fig. 5. The corresponding increase of population is observed also for other levels. In particular, a remarkable increase of population is observed for level 1, which is the key point for understanding of the dip in the delay dependence of PL intensity observed experimentally; see Fig. 4(a).

Figure 6 shows the integral PL intensity, I_{PL}, as a function of the delay between pulses, τ_{delay}, for two excitation powers with total power, $P^{(1)} + P^{(2)} < P_{th}$, where P_{th} is the threshold power for polariton lasing. Curves I_i represent the contribution of each transition term having form $W_{i-1}N_i(N_1 + 1)$ for $i = 2 \ldots 6$, into the total PL. As one can see from the figure, the modeling predicts a dip in the PL intensity at the small delays. It is clear from the discussion above that the dip is due to the increase of PL intensity at the delay increases up to several picoseconds.

Further increase of delay between the pulses gives rise to the depopulation of level 5 when the second pulse arrives. As a result the Bose-stimulated relaxation of levels 6 and 7 excited by the second pulse becomes less efficient and the nonradiative losses increase. This explains the decrease of PL intensity at delays $\tau = 10 \ldots 40$ ps; see Fig. 6(b). However, when the delay $\tau > 40$ ps, the population of the ground exciton

level is so large ($N_1 \ll 1$) that the direct Bose-stimulated relaxation from level 6 described by term $W_5 N_6(N_1 + 1)$ becomes an efficient pathway for the exciton relaxation to the ground level. Correspondingly, efficient depopulation of level 6 occurs that results in the decrease of nonradiative losses. These processes explain the appearance of a second peak at the delay dependence of PL intensity. The calculated behavior of total PL intensities at weak and strong pumping qualitatively reproduce the experimental results [compare with Fig. 4(a)].

VII. CONCLUSIONS

Present experiments and modeling shed light on the exciton dynamics in bosonic cascades, the pump-pump method being a powerful tool for the study of the fast relaxation dynamics at the nonresonant pumping. When the only one pump pulse is used for excitation, the relaxation occurs via one pathway. Using the second pulse allows one to switch the relaxation between different pathways depending on delay between the pulses which we demonstrate experimentally and through modeling. We have found a qualitative agreement between the theoretical model of a BCL in a PQW system and experimental results. Because the pump-pump method is based on strong nonlinearity of PL yield on the pump power, which is close to the threshold, we could not expect the quantitative agreement of the theory and the experiment. However, the modeling showed that there are two different pathways for relaxation in the system. The first pathway is the relaxation via cascade transitions, where all levels are being filled, and the second pathway is the direct transition from the pumped level to the ground one. By taking these pathways into account, the model may be generalized for larger number of levels or for other initial conditions. Taking into account the fact that minimum in the PL at zero delay occurs only if polaritons are exited on at least two adjacent levels, it is possible to explain the difference in PL for PQW and bare QW shown in Fig. 4: the levels in bare QW stand far from each other and polaritons are excited only at one energy level. Due to this there is no minimum at zero delay between pump pulses. However the relaxation process in the bare QW still may be described by the rate equations, but with different parameter values.

As a conclusion, this work shows potentiality of microcavities with embedded PQW for realization of bosonic cascade lasers.

ACKNOWLEDGMENTS

The authors thank Dr. Anton Nalitov for fruitful discussions. A.K. and E.C. acknowledge support through the EPSRC established career fellowship and EPSRC Hybrid Polaritonic Programme, A.K. is grateful for the financial support from the Russian Ministry of Science and Education (Contract No. 11.G34.31.0067) and RFBR Grant No. 15-59-30406. I.I. acknowledges the financial support of SPbU (Grant No. 11.38.213.2014). The authors also thank the SPbU Resource Center "Nanophotonics" (www.photon.spbu.ru) for the sample studied in the present work.

[1] A. Kavokin, Nat. Photon. **7**, 591 (2013).
[2] V. Savona, in *The Physics of Semiconductor Microcavities: From Fundamentals to Nanoscale Devices*, edited by B. Deveaud (Wiley-VCH Verlag GmbH & Co. KGaA, Weinheim, 2007), pp. 1–29.
[3] G. Weihs, H. Deng, R. Huang, M. Sugita, F. Tassone, and Y. Yamamoto, Semicond. Sci. Technol. **18**, S386 (2003).
[4] J. Kasprzak, M. Richard, S. Kundermann, A. Baas, P. Jeambrun, J. M. J. Keeling, F. M. Marchetti, M. H. Szymańska, R. André, J. L. Staehli, V. Savona, P. B. Littlewood, B. Deveaud, and L. S. Dang, Nature (London) **443**, 409 (2006).
[5] T. C. H. Liew, M. M. Glazov, K. V. Kavokin, I. A. Shelykh, M. A. Kaliteevski, and A. V. Kavokin, Phys. Rev. Lett. **110**, 047402 (2013).
[6] M. Tonouchi, Nat. Photon. **1**, 97 (2007).
[7] J. Faist, F. Capasso, D. Sivco, C. Sirtori, A. Hutchinson, and A. Cho, Science **264**, 553 (1994).
[8] A. A. Bogdanov and R. A. Suris, Phys. Rev. B **83**, 125316 (2011).
[9] R. F. Kazarinov and R. Suris, Sov. Phys. Semicond. **5**, 707 (1971).
[10] M. A. Kaliteevski and K. A. Ivanov, Tech. Phys. Lett. **39**, 91 (2013).
[11] J. Ulrich, R. Zobl, K. Unterrainer, G. Strasser, E. Gornik, K. D. Maranowski, and A. C. Gossard, Appl. Phys. Lett. **74**, 3158 (1999).
[12] M. Studer, G. Salis, K. Ensslin, D. C. Driscoll, and A. C. Gossard, Phys. Rev. Lett. **103**, 027201 (2009).
[13] M. Geiser, F. Castellano, G. Scalari, M. Beck, L. Nevou, and J. Faist, Phys. Rev. Lett. **108**, 106402 (2012).
[14] C. A. Duque and M. E. Mora-Ramos, Superlattices Microstruct. **54**, 61 (2013).
[15] H. V. Phuc, N. N. Hieu, L. Dinh, and T. C. Phong, Opt. Commun. **335**, 37 (2015).
[16] T. Yan, J. He, W. Yang, K. Rajabi, W. Chen, J. Wu, X. Kang, G. Zhang, and X. Hu, Phys. Status Solidi A: Appl. Mater. Sci. **212**, 925 (2015).
[17] R. Colombelli, C. Ciuti, Y. Chassagneux, and C. Sirtori, Semicond. Sci. Technol. **20**, 985 (2005).
[18] S. De Liberato and C. Ciuti, Phys. Rev. Lett. **102**, 136403 (2009).
[19] A. V. Kavokin, I. A. Shelykh, T. Taylor, and M. M. Glazov, Phys. Rev. Lett. **108**, 197401 (2012).
[20] E. del Valle and A. Kavokin, Phys. Rev. B **83**, 193303 (2011).
[21] I. G. Savenko, I. A. Shelykh, and M. A. Kaliteevski, Phys. Rev. Lett. **107**, 027401 (2011).
[22] K. V. Kavokin, M. A. Kaliteevski, R. A. Abram, A. V. Kavokin, S. Sharkova, and I. A. Shelykh, Appl. Phys. Lett. **97**, 201111 (2010).
[23] A. Tzimis, A. V. Trifonov, G. Christmann, S. I. Tsintzos, Z. Hatzopoulos, I. V. Ignatiev, A. V. Kavokin, and P. G. Savvidis, Appl. Phys. Lett. **107**, 101101 (2015).
[24] M. Cardona, *Solid State Physics: Modulation Spectroscopy* (Academic Press, New York, 1969).

[25] E. L. Ivchenko, *Optical Spectroscopy of Semiconductor Nanostructures* (Springer, Berlin, 2004).
[26] A. V. Trifonov, S. N. Korotan, A. S. Kurdyubov, I. Y. Gerlovin, I. V. Ignatiev, Y. P. Efimov, S. A. Eliseev, V. V. Petrov, Y. K. Dolgikh, V. V. Ovsyankin, and A. V. Kavokin, Phys. Rev. B **91**, 115307 (2015).
[27] R. Butté, G. Delalleau, A. I. Tartakovskii, M. S. Skolnick, V. N. Astratov, J. J. Baumberg, G. Malpuech, A. Di Carlo, A. V. Kavokin, and J. S. Roberts, Phys. Rev. B **65**, 205310 (2002).
[28] H. Mathieu, P. Lefebvre, J. Allegre, B. Gil, and A. Regreny, Phys. Rev. B **36**, 6581 (1987).
[29] T. C. Damen, J. Shah, D. Y. Oberli, D. S. Chemla, J. E. Cunningham, and J. M. Kuo, Phys. Rev. B **42**, 7434 (1990).
[30] V. P. Kochereshko, M. V. Durnev, L. Besombes, H. Mariette, V. F. Sapega, A. Askitopoulos, I. G. Savenko, T. C. H. Liew, I. A. Shelykh, A. V. Platonov, S. I. Tsintzos, Z. Hatzopoulos, P. G. Savvidis, V. K. Kalevich, M. M. Afanasiev, V. A. Lukoshkin, C. Schneider, M. Amthor, C. Metzger, M. Kamp, S. Hoefling, P. Lagoudakis, and A. Kavokin, Sci. Rep. **6**, 20091 (2016).
[31] J. Bloch, B. Sermage, M. Perrin, P. Senellart, R. André, and L. S. Dang, Phys. Rev. B **71**, 155311 (2005).
[32] L. Schultheis, J. Kuhl, A. Honold, and C. W. Tu, Phys. Rev. Lett. **57**, 1635 (1986).
[33] O. Heller, J. Tignon, J. Martinez-Pastor, P. Roussignol, G. Bastard, M. Maaref, V. Thierry-Mieg, and R. Planel, Nuovo Cimento D **17**, 1493 (1995).
[34] G. Khitrova, H. M. Gibbs, F. Jahnke, M. Kira, and S. W. Koch, Rev. Mod. Phys. **71**, 1591 (1999).
[35] G. Bongiovanni, A. Mura, F. Quochi, S. Gürtler, J. L. Staehli, F. Tassone, R. P. Stanley, U. Oesterle, and R. Houdré, Phys. Rev. B **55**, 7084 (1997).
[36] H. Deng, H. Haug, and Y. Yamamoto, Rev. Mod. Phys. **82**, 1489 (2010).
[37] A. Kavokin, *Cavity Polaritons*, Thin Films and Nanostructures Vol. 32 (Elsevier/Academic Press, Amsterdam, 2003).